Magnetic excitations and soft-mode transition in the quasi-one-dimensional mixed-spin antiferromagnet Pr_2BaNiO_5

A. Zheludev, J. M. Tranquada, and T. Vogt
Brookhaven National Laboratory, Upton, New York 11973-5000

D. J. Buttrey
University of Delaware, Newark, Delaware 19716

(Received 8 April 1996)

Neutron diffraction and inelastic neutron scattering were used to investigate three-dimensional (3D) antiferromagnetic ordering and magnetic excitations in Pr_2BaNiO_5, a quasi-1D mixed-spin antiferromagnet. Three distinct features of the magnetic excitation spectrum were observed above the Néel temperature T_N: a strongly 1D gap excitation propagating on the Ni chains, a single-ion crystal-field transition associated with Pr^{3+}, and a strongly temperature-dependent mixed Pr-Ni magnetic-exciton band. Ni-chain modes persist in the 3D ordered phase, and the energy gap increases with decreasing T below T_N. The magnetic-exciton band undergoes a complete softening at the antiferromagnetic zone center as T_N is approached from above, driving the magnetic phase transition. [S0163-1829(96)08433-0]

I. INTRODUCTION

Interest in low-dimensional magnetism has been greatly renewed by the theoretical work of Haldane,[1] who predicted that an integer-spin Heisenberg antiferromagnetic (AF) chain should have a *singlet* ground state, exponentially decaying correlations, and a *gap* in the magnetic excitation spectrum. The Haldane conjecture is now supported by numerous numerical results.[2–5] Several examples of real quasi-one-dimensional (quasi-1D) systems with a Haldane gap have been studied by now (for a comprehensive reference list see Ref. 6). Since the first discovery of the Haldane gap in $CsNiCl_3$,[7–10] most of the experimental work was done on NENP (Refs. 6, 11 and 12) and other organometallic compounds,[13–17] which often have extremely weak interchain interactions and are therefore good examples of 1D systems.

Darriet and Regnault[18] and DiTusa *et al.*[19,20] were the first to observe a Haldane gap in a metal oxide compound, namely, Y_2BaNiO_5. Y_2BaNiO_5 is a member of a large family of linear-chain compounds with the general formula L_2BaNiO_5 (L=Y, Pr, Nd, Sm, Eu, Gd, Tb, Dy, Ho, Er, and Tm).[21,22] In these species stacks of distorted NiO_6 octahedra share apical oxygens to form antiferromagnetic ($S=1$ for Ni^{2+}) chains along the a axis of the orthorhombic structure [space group *Immm*, Fig. 1(a)]. In the case L=Y (nonmagnetic L) the interaction between the Ni chains is negligible. No long-range magnetic order is observed at low temperatures and the system appears to be a perfect Haldane-gap antiferromagnet.[18–20] In all other L_2BaNiO_5 species L is a magnetic rare-earth ion, which, interacting with the Ni^{2+} spins, leads to 3D AF ordering, with Néel temperatures ranging 24–50 K (see Ref. 23 and references therein).

It is well known that, provided the intrachain interactions are dominant, the onset of 3D long-range magnetic order does not eliminate Haldane-like behavior above the Néel temperature T_N.[7–10,24–26] Nevertheless, Y_2BaNiO_5, being a near-perfect model 1D system, appeared to be of a greater immediate fundamental interest than the other L_2BaNiO_5 species, which were largely ignored, as far as the spin dynamics is concerned. The present work deals with neutron scattering studies of Pr_2BaNiO_5, a recently synthesized member of the L_2BaNiO_5 family.[27] Our main goal was to

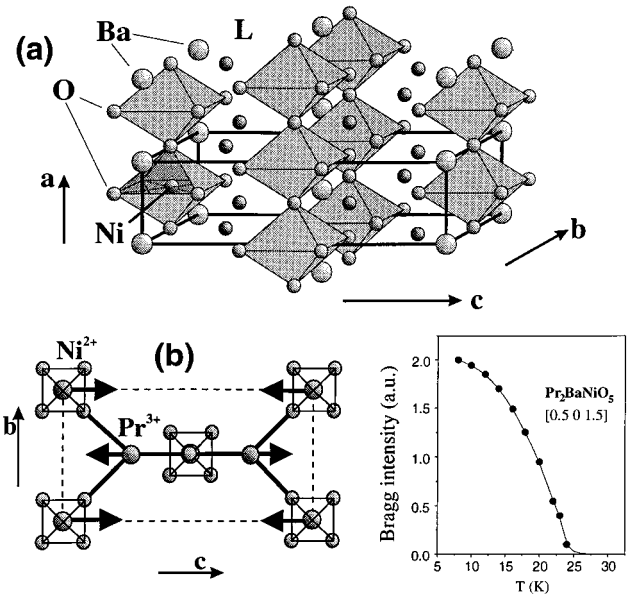

FIG. 1. (a) L_2BaNiO_5 chemical unit cell, showing the NiO_6 octahedra stacked along the a crystallographic axis. (b) Structural relation between the Ni and rare-earth sites in Pr_2BaNiO_5. The heavy lines show the possible Ni-Pr and Pr-Pr superexchange pathways. The arrows indicate the orientation of ordered moments in the 3D antiferromagnetic phase. (c) Temperature dependence of (0.5,0,1.5) magnetic Bragg peak intensity measured in Pr_2BaNiO_5 single crystal.

observe Haldane-like gap excitations in this material and investigate how they are influenced by the antiferromagnetic phase transition. We demonstrate that 1D Ni-chain magnetic gap excitations are indeed present in Pr_2BaNiO_5 above the Néel temperature $T_N = 24$ K and persist in the low-temperature 3D antiferromagnetic phase. Unlike what is seen in $CsNiCl_3$,[7–10,25] an extensively studied system with Haldane gap modes and 3D AF ordering below $T_N = 4.8$ K, the Ni-chain modes in Pr_2BaNiO_5 do not soften at the transition temperature and survive as 1D gap excitations in the 3D phase.

What makes Pr_2BaNiO_5 especially interesting and, in a way, exotic, is the unusual mechanism of magnetic ordering. Due to the low site symmetry, Pr^{3+} ions in Pr_2BaNiO_5 should have a nonmagnetic ground state. We find that the onset of 3D Néel order is driven by a temperature-dependent dispersion of a Pr-Ni magnetic-exciton band. The finite moment on Pr is thus induced by exchange interactions with other magnetic ions. We simultaneously observe spin excitations of the Ni-O chains that have a gap consistent with Haldane's conjecture and a separate Pr-Ni mixed-spin mode. Long-range magnetic order is induced by interactions between two nominally nonmagnetic subsystems: quenched-moment rare-earth ions and quantum-disordered spin chains.

II. EXPERIMENT

Single crystals of the linear-chain phase of Pr_2BaNiO_5 were prepared by skull melting, as described elsewhere.[27] The largest single-crystal sample obtained ($4\times4\times4$ mm^3), was just large enough for inelastic neutron scattering experiments. As mentioned above, the crystal structure is orthorhombic, space group $Immm$, a being the Ni-chain direction, with the room-temperature cell constants $a = 3.85$ Å (intrachain Ni-Ni distance), $b = 5.96$ Å, and $c = 11.70$ Å.

Single-crystal magnetic neutron diffraction data were collected at the H6 spectrometer at the High Flux Beam Reactor (HFBR) at Brookhaven National Laboratory in a four-circle geometry using a $\lambda = 1.1$ Å neutron wavelength. Inelastic neutron scattering experiments were carried out at the H4M, H7, and H8 triple-axis spectrometers. For the latter the sample was mounted with the (0,1,0) reciprocal plane parallel to the scattering plane of the spectrometer, making $(h,0,l)$-type wave vectors accessible. In all cases the use of standard or two-stage Displex refrigerators allowed us to perform the measurements in the temperature range 5–100 K.

For the inelastic measurements several experimental setups were exploited. PG (pyrolitic graphite) (0,0,2) reflections were used for monochromator and analyzer. In most cases a fixed final neutron energy $E_f = 14.7$ meV was used, with a PG filter positioned after the sample to eliminate higher-order beam contamination. To meet the conflicting needs of resolution and intensity, 40′-40′-40′-40′ (setup A) and 40′-80′-80′-40′ (setup B) collimations were utilized. Alternatively, fixed incident-energy experiments ($E_i = 30.5$ meV for setup C and $E_i = 41$ meV for setup D) were performed using 40′-80′-40′-80′ collimations and a PG filter in front of the sample.

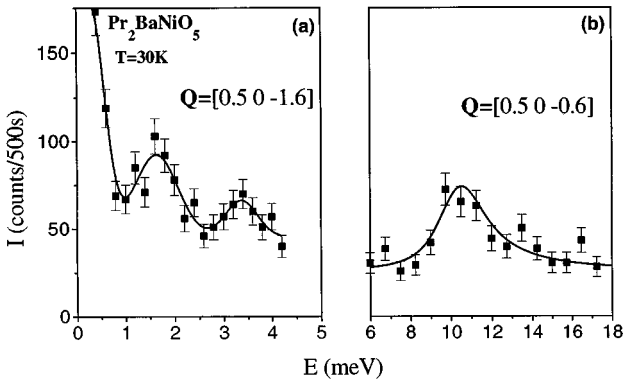

FIG. 2. Constant-Q scans taken at 30 K in the vicinity of the 3D AF zone centers $\mathbf{Q} = (0.5,0,-1.6)$ (a) and $\mathbf{Q} = (1.5,0,-0.6)$ (b) in Pr_2BaNiO_5. The 11 meV peak has also been observed at $\mathbf{Q} = (0.5,0,-1.6)$, but appears weaker due to a strong defocusing at this position. The solid lines are guides to the eye.

III. RESULTS AND DATA TREATMENT

Magnetic order is revealed by the appearance of Bragg reflections of the type $((2m+1)/2, 0, (2n+1)/2)$ below the Néel temperature $T_N = 24$ K.[28] The temperature dependence of the (0.5,0,1.5) peak is shown in Fig. 1(c). The analysis of diffraction data, collected at $T = 8$ K, shows that Pr_2BaNiO_5 has basically the same type of collinear magnetic structure as Nd_2BaNiO_5, studied previously by Sachan *et al.*[23] Both Ni and Pr ordered moments are in the (a,c) plane and are nearly perpendicular to the Ni-O chains, forming an angle of $\approx 9.5°$ with the c crystallographic axis. At $T = 8$ K the ordered moments on Ni^{2+} and Pr^{3+} sites were found to be $1.1\mu_B$ and $1.3\mu_B$, respectively. A more detailed analysis of the crystal and magnetic structure will be published elsewhere.[27]

Figure 1(b) schematically shows the structural relation between the Pr and Ni sites. Several Ni-O-Pr superexchange pathways may exist in the structure. The most potent one links the Ni sites to rare-earth ions via the equatorial oxygen positions of the NiO_6 octahedra, as shown in Fig. 1(b) with solid lines. The (antiferromagnetic) effective Ni-Pr exchange integral is expected to be relatively large, thanks to the favorable Ni-O-Pr bond angle ($\approx 180°$). Other Ni-O-Pr superexchange routes (not shown) involve the apical or equatorial oxygens of the NiO_6 octahedra and couple each Pr ion to two adjacent Ni sites in the nearest Ni-O chain. These bonds are frustrated by the antiferromagnetic correlations which exist within the Ni chains. In addition, the corresponding interactions are expected to be small (Ni-O-Pr angles close to 90°). The 3D spin network is completed by nearest-neighbor Pr ions that are coupled via the apical oxygen of the nearest Ni-O chain [also shown in Fig. 1(b)].

Typical inelastic constant-Q scans, collected near the 3D AF reciprocal-space points at $T = 30$ K (above $T_N = 24$ K) using setups A and B, are shown in Fig. 2. They demonstrate three distinct features of the magnetic excitation spectrum. As will be argued in the following sections, the peak seen at $\hbar\omega \approx 11$ meV corresponds to strongly 1D Haldane-like gap modes in the Ni-chain subsystem (although this mode has a strong dispersion, it will be referred to as the ''11 meV''

excitation), without contributions from Pr moments. The ≈ 3.5 meV feature is identified as a predominantly single-ion crystal-field (CF) transition in Pr^{3+}. Finally, the low-energy peak is associated with a mixed-spin magnetic-exciton band, propagating on both the Ni and Pr sites.

A. Ni-chain gap excitations

In this section we first give a qualitative discussion of the observed Q dependence in the Haldane-like Ni-chain excitations at $T=30$ K. This is followed by subsections describing the quantitative analysis of the experimental data and the measured temperature dependence.

1. Q dependence

True Haldane-gap excitations carry a spin of $S=1$ and are therefore threefold degenerate. The triplet is usually split by single-ion anisotropy. Since Darriet and Regnault first published their results for Y_2BaNiO_5,[18] the Ni-site anisotropy was believed to be of easy-plane character and the Haldane triplet split into a doublet of modes polarized perpendicular to the Ni chains with $\Delta_\perp \approx 10$ meV and a singlet excitation polarized along the a crystallographic axis with $\Delta_\parallel \approx 17$ meV. More recent studies[29,30] unambiguously show that the anisotropy is of easy-axis type, and the longitudinal mode is found at much lower energy, with $\Delta_\parallel \approx 7$ meV.

The cummulative polarization factor for the inelastic intensity in the two transverse-polarized branches is given by[18,6]

$$P_\perp(\mathbf{Q}) = 1 + \frac{1}{1+(Q_\perp/Q_\parallel)^2}, \tag{1}$$

where $Q_\parallel$ and $Q_\perp$ stand for the components of the scattering vector along and perpendicular to the chain direction, respectively. If the sample is mounted on a three-axis spectrometer with the (a,c) plane horizontal, the mode polarized along the c axis has a polarization factor given by the second term on the right-hand side of Eq. (1), and the intensity is therefore largest near $Q_\perp = 0$. The other transverse excitation (polarized along b) should have no polarization dependence. The polarization factor for the longitudinal branch is given by

$$P_\parallel(\mathbf{Q}) = \frac{1}{1+(Q_\parallel/Q_\perp)^2}, \tag{2}$$

and the measurements have to be performed at large $Q_\perp/Q_\parallel$ To satisfy this condition and still remain on the 1D AF zone-center planes one has to go to large values of $Q_\perp$.

In Pr_2BaNiO_5 at $T=30$ K the ''11 meV'' excitation has a strongly anisotropic dispersion that is parabolic about the 3D AF reciprocal-space points. The dispersion was found to be very steep along the Ni-chain axis a^*. The energy-integrated intensity decreases rapidly as one moves away from the half-integer-h planes (1D AF zone-center planes) in reciprocal space. This is illustrated in Figs. 3(a), 3(b), and 3(c), which show constant-Q scans measured using experimental setup B at $\mathbf{Q}=(1.5,0,-0.2)$, $(1.52,0,-0.2)$, and $(1.53,0,-0.2)$. The dispersion along the c axis is small [Figs. 3(a) and 3(d)]. The inelastic intensity shows only a monotonous decrease in this direction (Fig. 4). Although this $Q_\perp$ dependence is largely

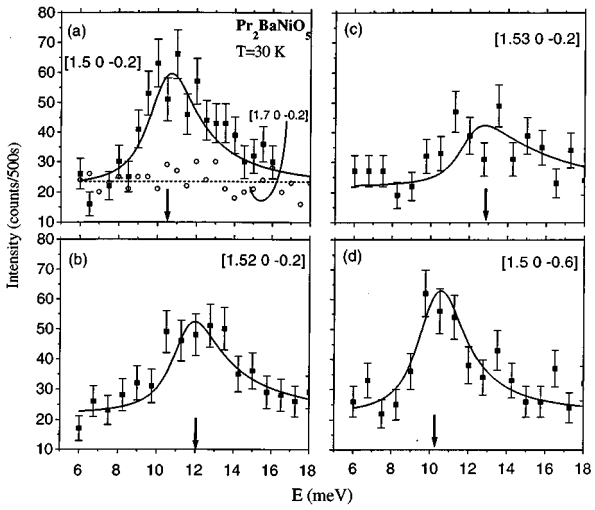

FIG. 3. Constant-Q scans measured in Pr_2BaNiO_5 single-crystal sample at $T=30$ K at several wave vectors close to the $(1.5,k,l)$ 1D zone-center plane. The peak corresponds to 1D Haldane-like gap modes propagating on the Ni sites. Open circles and the dashed line represent the background measured at $\mathbf{Q}=(1.70-0.2)$. The solid lines show fits to the model cross section obtained using three-axis deconvolution analysis and the model cross section defined by Eq. (4) and Eq. (3).

due to the combined effects of resolution defocusing and magnetic form factor for Ni^{2+} (see below), the broad peak at $Q_\perp = 0$ indicates that we are dealing with transverse-polarized excitations. It is very important to note that no 3D-*structure factor*-like dependence (which one could expect if both Ni and Pr spins were contributing) was found in the ''11 meV'' peak. The observed Q dependence of the excitation energy and intensity is totally consistent with our expectations for 1D Haldane-like transverse-polarized gap modes propagating on the Ni chains. This is supported by the observation that the gap $\Delta \approx 11$ meV in Pr_2BaNiO_5 is close to the transverse Haldane gap $\Delta \approx 10$ meV in Y_2BaNiO_5.

We have also attempted to observe the longitudinal-polarized Ni-chain mode in Pr_2BaNiO_5 around $(0.5,0,-4)$ and $(0.5,0,-6)$, but without any success. Although this excitation may indeed be absent, it may also be simply very difficult to see in the small sample we have. Indeed, in the geometry required to observe the longitudinal mode (large $Q_\perp$) magnetic inelastic intensities suffer a severe attenuation caused by the magnetic form factor and resolution effects due to the crystal mosaic.[17]

2. Analysis of the dispersion relation

To quantitatively analyze the measurements, we adopt a form of the dynamic structure factor $S(\mathbf{q},\omega)$ successfully applied in the study of other Haldane systems:[6,17]

$$S(\mathbf{q},\omega) = \frac{S_0\xi/\Gamma}{1+q_\parallel^2\xi^2+(\omega-\omega_\mathbf{q})^2/\Gamma^2}. \tag{3}$$

Here $\mathbf{q}$ is measured relative to a 1D AF point $((2n+1)/2,k,l)$ (integer n, k, and l) and $\parallel$ denotes the component along the chain axis; ξ is the intrachain spin correla-

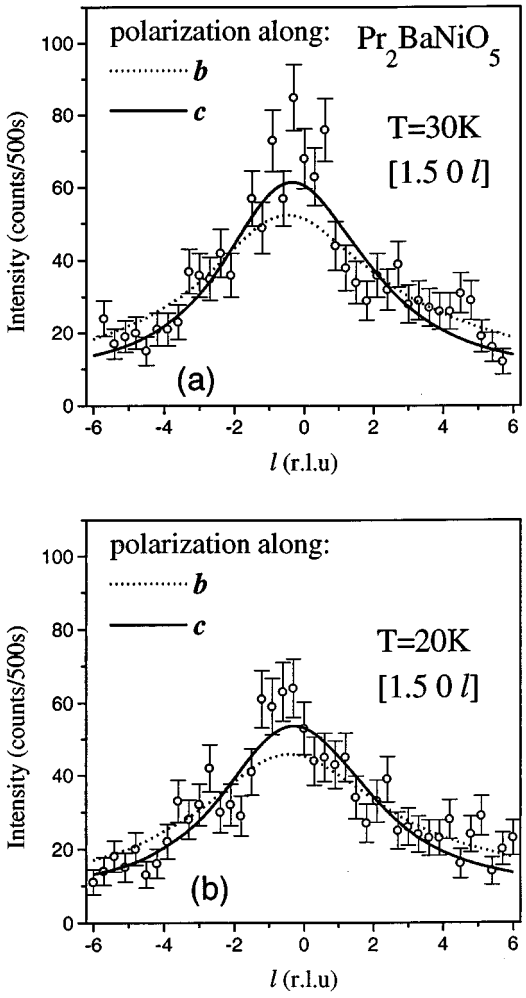

FIG. 4. Constant-energy l scan for $\mathbf{Q}=(1.5,0,l)$, $\hbar\omega=11$ meV measured in Pr_2BaNiO_5 at $T=30$ K (a). A similar scan collected at $T=20$ K, $\hbar\omega=12$ meV (b). The lines represent the Q dependence expected for Haldane-gap excitations polarized along the b (dotted line) and c (solid line) crystallographic axes.

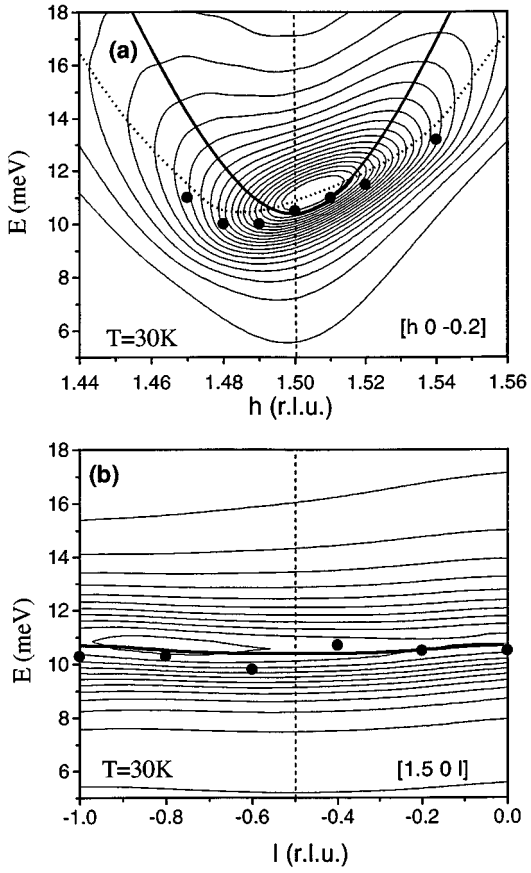

FIG. 5. Constant-intensity contours in $(h,(\hbar\omega))$ and $(l,(\hbar\omega))$ space for the Ni-chain mode, simulated using Eqs. (4) and (3), the refined parameter values, and the known spectrometer resolution function. The heavy line shows the experimental dispersion relation. The dotted line in panel (a) shows the calculated positions of intensity maxima in constant-Q scans. Solid circles on both panels mark the actually observed peak positions (Pr_2BaNiO_5, $T=30$ K).

tion length, Γ the intrinsic energy width, and S_0 is an overall scale factor. The dispersion is approximated by

$$(\hbar\omega_{\mathbf{q}})^2=\Delta^2+c_0^2q_\parallel^2+\Delta_E^2[1+\cos(cq_\perp)]^2/4, \qquad (4)$$

where Δ is the value of the Haldane gap, c_0 is the spin-wave velocity along the chains, and Δ_E is related to the magnitude of the dispersion along c^*. After convoluting the cross section (3) with the four-dimensional $(E,\mathbf{Q})$ spectrometer resolution function, parameter values were determined by a global least-squares fit to a series of constant-$\mathbf{Q}$ scans measured at $T=30$ K for wave vectors $\mathbf{Q}=(h,0,l)$ in the range $1.46\leqslant h\leqslant 1.54$ and $-1\leqslant l\leqslant 0$ using collimation setup B. A fitting to 240 experimental data points converged to the following set of parameters: $\Delta=10.4(0.1)$ meV, $1/\xi=0.08(0.03)$ Å^{-1}, $\Gamma=0.9(0.1)$ meV, $c_0=200(11)$ meV Å, and $\Delta_E=2.5(0.8)$ meV, with $\chi^2=0.95$. The solid lines in Fig. 3 show examples of intensity profiles calculated from the refined parameter values.

Figure 5 shows the dispersion relation (heavy line) and constant-intensity contours (thin line) calculated using the refined parameter values and convoluted with the three-axis resolution function, illustrating just how strong the resolution effects are. The calculated positions of intensity maxima in constant-Q scans are represented by the dotted line in Fig. 5(a). The solid circles in both Figs. 5(a) and 5(b) stand for the actually observed peak positions.

After taking into account quantum renormalization corrections for the spin-wave velocity of an $S=1$ linear Heisenberg AF system, we obtain an estimate $J=c_0/(2.7a)\approx 223$ K for the effective intrachain Ni-Ni exchange constant. This value is slightly smaller than $J=285$ K for Y_2BaNiO_5.[31] It is very important to note that the relation $\Delta\approx c_0/\xi$, a universal property of Haldane-gap systems,[3–5] is qualitatively satisfied by the refined parameter values. The measurements of the transverse dispersion provide a rough estimate[6] for the effective interchain exchange constant $|J'|\approx 5\times 10^{-4}|J|$ at $T=30$ K, which is at least one order of magnitude too small to induce any long-range order.[25] This is indeed surprising, since the material *does* order in three dimensions at $T_N=24$ K.

3. Analysis of constant-energy scans and polarization

The analysis of constant-E scans that span a wide range of momentum transfers (like those shown on Fig. 4) requires taking into account the Ni^{2+} magnetic form factor $|f(Q)|^2$ and the magnon-polarization factor $P_\perp(\mathbf{Q})$ for the scattering cross section of unpolarized neutrons. Equations (3), (4), and each of the right-hand-side terms in Eq. (1) combined with the Ni^{2+} form factor,[32] the 4D resolution function, and the parameters previously determined from the analysis of constant-Q scans (see above), were used to fit the data collected in the constant-E scan at $\hbar\omega=11$ meV, $Q=(1.5,0,l)$, shown in Fig. 4. An overall scaling factor was the only adjustable parameter. Since the $Q_\perp$ dependence of the inelastic intensity is mostly due to resolution and form factor effects, the quality and quantity of available data prevent us from unambiguosly separating the contributions from modes polarized along the b and c axes. Using polarization factors for either of these modes produces fits which are in reasonable agreement with experiment (Fig. 4, solid and dashed lines). We do note, however, that the $Q_\perp$ scan collected at $T=30$ K [Fig. 4(a)] is more sharply peaked around $Q_\perp=0$ and appears to be quantitatively inconsistent with the profile calculated for a single mode polarized along b, suggesting a significant contribution from a c-polarized excitation. A more reliable polarization analysis requires the use of a polarized neutron beam. Unfortunately, our sample is not large enough to perform a polarized-neutron experiment, in which the incident flux is at least an order of magnitude smaller then when using unpolarized neutrons.

4. Temperature dependence

Figure 6 shows the observed evolution of the ''11 meV'' excitation in Pr_2BaNiO_5 as the sample was cooled down through the transition temperature T_N. The ''11 meV'' feature is *still present in the ordered phase*. Its intensity decreases on cooling with no change in energy width. The peak energy *increases* with decreasing temperature below T_N. At $T>T_N$ the opposite behavior is observed: The peak shifts to slightly higher energies, broadens, and weakens with increasing temperature. It could not be observed at $T>75$ K.

The data were analyzed by fitting the cross section (3) convoluted with the spectrometer resolution function to constant-Q scans measured using setup B at different temperatures. The parameters c_0 and ξ were assumed to be temperature independent and the previously obtained 30 K values were used. These constants are needed only to take proper account of the resolution effects, and the assumption should not affect the fitting results. Since only individual scans at the same $\mathbf{Q}$ position were analyzed, the parameter Δ_E was set to be zero. Therefore, the refined gap value, plotted against temperature in Fig. 7(a), accounts for both the actual energy gap at the dispersion minimum (at the 3D AF zone center) and the effect of a finite dispersion perpendicular to the chain direction. It is important to emphasize that the transverse dispersion shows no temperature dependence, i.e., remains very small even in the ordered phase [Fig. 7(a)].

The temperature dependence of the energy-integrated intensity in the Ni-chain modes is shown in Fig. 7(b). Above T_N a gradual decrease of intensity with increasing temperature is observed. This behavior is typical of Haldane-gap antiferromagnets (see, for example, Ref. 13). In contrast, the intensity decreases abruptly on cooling below $T_N=24$ K, roughly by a factor of 2, but rapidly levels off and remains constant below $T=20$ K.

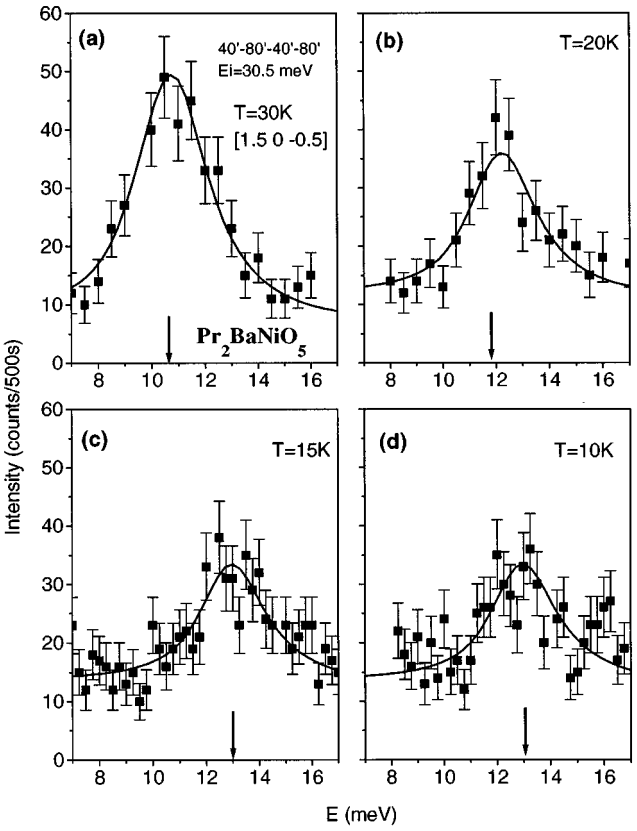

FIG. 6. Example constant-Q scans showing the Ni-chain gap excitation in Pr_2BaNiO_5 at several temperatures above and below the ordering temperature $T_N=24$ K. The solid lines represent fits obtained with three-axis deconvolution analysis.

The $Q_\perp$ dependence of the inelastic intensity in the ordered phase [Fig. 4(b)] is very similar to that observed above the Néel temperature [Fig. 4(a)]. The only visible difference is that the profile appears to be less sharply peaked around $Q_\perp=0$.

B. Single-ion crystal-field excitation in Pr^{3+}

We now turn to the excitation represented by the peak centered at $\Delta_{CF}\approx 4$ meV in the constant-Q scan shown in Fig. 2. In the entire temperature range studied, this mode shows practically no dispersion either along or perpendicular to the Ni chains. This is illustrated by Fig. 8, which shows typical constant-Q scans at $\mathbf{Q}=(h,0,-1.5)$ measured for several values of h at $T=30$ K. The solid lines show empirical Gaussian fits with a sloping background (dotted lines). The energy-integrated intensity of the ''4 meV'' feature shows only a smooth form-factor-like decrease at large momentum transfers. All of the above, together with the fact that no similar excitations were observed in Nd_2BaNiO_5 (Ref. 33) and Y_2BaNiO_5 (Refs. 19 and 20), suggests that the 4 meV mode corresponds to a single-ion (dispersionless) crystal-field transition in Pr.

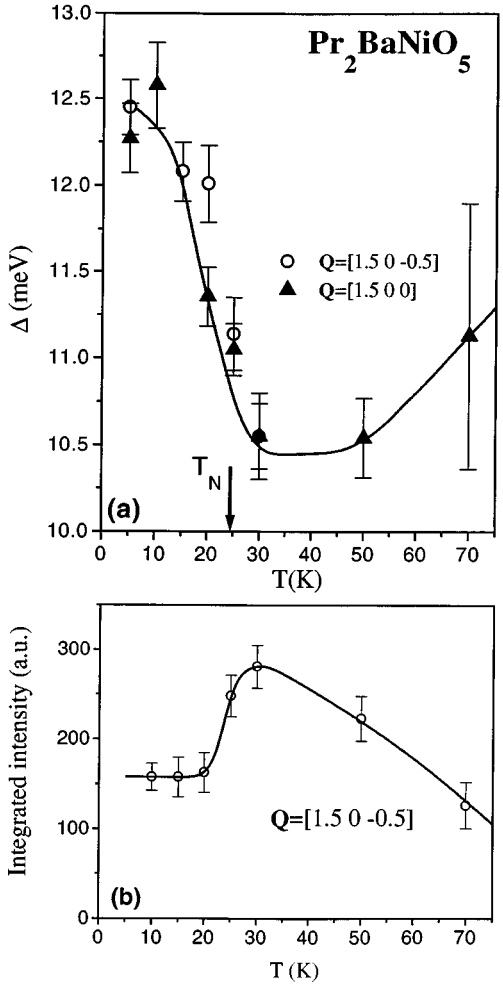

FIG. 7. Measured temperature dependences of the energy gap in the Ni-chain modes in Pr_2BaNiO_5 (a) and their energy-integrated intensity (b). The solid lines are a guide to the eye.

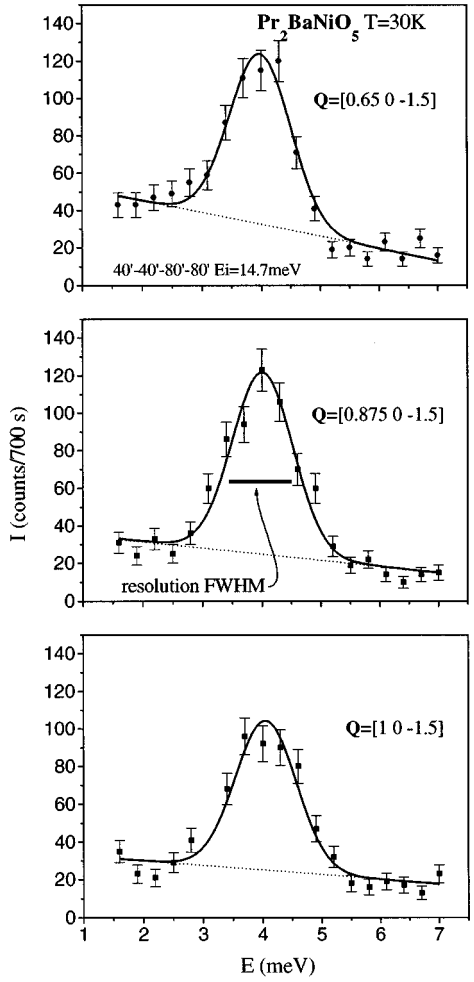

FIG. 8. Example constant-Q scans showing the single-ion crystal-field excitation in Pr_2BaNiO_5 at different wave vectors, $T=30$ K. The solid lines are empirical Gaussian fits with a sloping background (dotted lines) .

The energy-integrated intensity in the CF excitation is plotted against temperature in Fig. 9. As expected for a single-ion CF transition, the cross section decreases rapidly with increasing T. The degeneracy of the nine $J=4$ Pr levels is completely removed by the low symmetry of the crystal environment. This allows for a multitude of CF transitions and our data are not sufficient to assign the observed feature to any particular one. In any case a singlet-to-singlet transition is expected. As a reference, the solid line in Fig. 9 shows the behavior expected for a singlet-singlet excitation in a two-level system. The obvious disagreement with experiment is most likely due to the presence of several low-energy CF levels that are ''hidden'' from neutron scattering experiments by selection rules. Alternatively, the ''4 meV'' peak may actually represent several overlapping modes. No temperature-induced broadening is observed in the single-ion CF excitation in Pr_2BaNiO_5 and the peak remains resolution limited between 5 and 150 K. The excitation energy shows only a small T dependence, decreasing slightly with temperature (Fig. 10, open circles).

C. Mixed Pr-Ni magnetic-exciton band

Perhaps the most interesting finding of this work is the lower-energy feature centered at ≈ 1.5 meV in the energy scan shown in Fig. 2. Near the AF zone centers this mode is observed only at $T>T_N$, has a highly anisotropic dispersion, and shows a strong temperature dependence in both dispersion and energy-integrated intensity.

1. Structure-factor dependence

The key feature of the low-energy excitation is the strong **Q** dependence of its cross section. The energy-integrated intensity of the 1.5-meV AF zone-center peak measured in several Brillouin zones at $T=30$ K follows the intensity pattern of the magnetic Bragg peaks observed at 10 K, as shown in Table I. This result indicates that the $((2m+1)/2,0,(2n+1)/2)$ (m,n integer) eigenvectors of the low-energy band are similar to the structure factor of the ordered state, with comparable amplitudes coming from Pr and Ni. On the other hand, the absence of similar excitations in the otherwise similar Nd_2BaNiO_5 (Ref. 33) suggests that the mode is associated with a crystal-field transition in Pr. As will be discussed below, this mode acquires a pronounced dispersion and structure-factor dependence due to the exchange coupling between Ni and Pr spins.

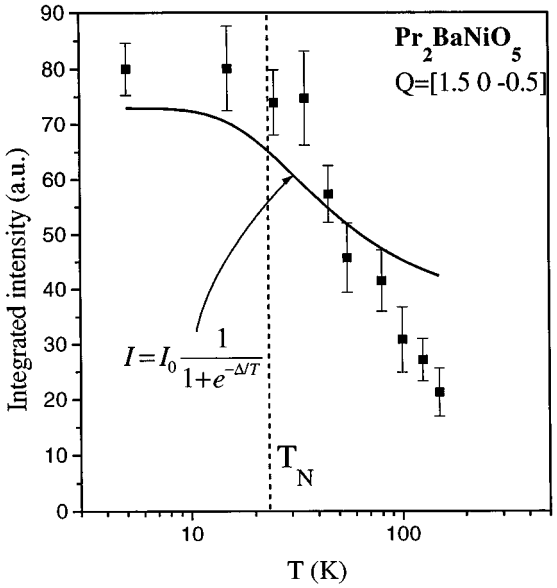

FIG. 9. Measured temperature dependence of the energy-integrated intensity in the single-ion crystal-field excitation in Pr_2BaNiO_5. The solid line shows the expected behavior for a singlet-singlet transition in a two-level system.

2. Dispersion at $T=30$ K

Magnetic excitations of dual nature (a mixture of single-ion CF transitions and spin waves with a substantial dispersion) are known as magnetic excitons and have been studied previously in several systems including Pr metal[34–36] and

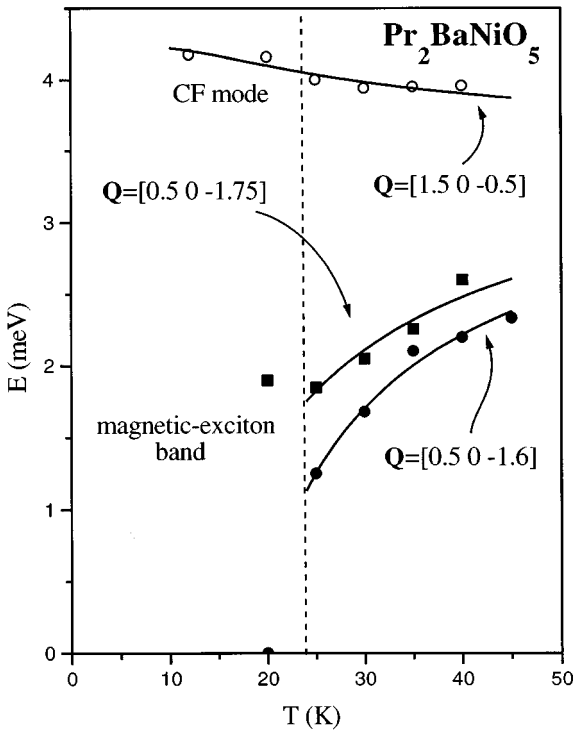

FIG. 10. Measured temperature dependence of the excitation energy in the single-ion crystal-field (open circles) and magnetic-exciton (solid circles) branches in Pr_2BaNiO_5.

TABLE I. Comparison of inelastic intensities in the magnetic-exciton band measured at several 3D antiferromagnetic zone centers at $T=30$ K for $\hbar\omega=1.8$ meV to the intensities of corresponding magnetic Bragg peaks measured at $T=10$ K.

$(2h\ 0\ 2l)$	1.8 meV (a.u.)	$\lvert F^2\rvert$ (10^{-24} cm)
($\bar{1}$ 0 3)	246(29)	2.82
(3 0 3)	133(25)	2.18
($\bar{1}$ 0 1)	38(21)	0.22
($\bar{1}$ 0 7)	31(21)	0.01
($\bar{3}$ 0 1)	30(21)	0.09
(3 0 9)	32(25)	0.75
($\bar{5}$ 0 1)	40(20)	0.09
($\bar{5}$ 0 3)	175(27)	1.66
(1 0 9)	0(25)	0.01

Pr_2CuO_4.[37] The energy of a single-ion CF excitation can be lowered by intersite exchange interactions. This introduces dispersion of the excitation bands, which in real space may be viewed as a single-ion excitation hopping from site to site.

The dispersion in the lower-energy magnetic-exciton band was investigated in the vicinity of $\mathbf{Q}=(0.5,0,-1.5)$. Several typical constant-Q scans, collected at $T=30$ K for different wave vectors, are shown in Fig. 11. The scans were analyzed by fitting the raw data with empirical Gaussian profiles. For each scan three Gaussians were used: one to account for incoherent scattering at $\hbar\omega=0$, one for the single-ion CF transition centered at $\hbar\omega=4$ meV, and one for the magnetic-exciton branch itself. Examples of such fits are represented by dashed lines in Fig. 11. The component relevant to the magnetic-exciton band is hatched. For the lack of a well-parametrized theoretical model cross section describing the low-energy mode, no resolution-function deconvolution analysis was performed. The dispersion has a global minimum at the 3D AF points $((2m+1)/2,0,((2n+1)/2)$, as shown in Figs. 12 and 13. The solid line in Fig. 12 is a guide to the eye. Perpendicular to the chain axis (Fig. 12) the dispersion is relatively small, but significantly larger than that in the Ni-chain modes. For wave vectors close to $\mathbf{Q}=(h,0,(2n+1)/2)$ (h,n integer) the experimental energy resolution prevents us from resolving the magnetic excitons and the single-ion CF transition at $\hbar\omega=4$ meV. The dispersion along the Ni-chain axis was found to be significantly steeper than in the transverse direction (Fig. 13). Similarly to what was seen in the Ni-chain mode, the intensity decreases rapidly as the scattering vector deviates from the 1D AF zone-center planes. The apparent lack of symmetry about $h=0.5$ is an artifact due to ''focusing'' effects associated with the resolution function. The longitudinal dispersion relation was analyzed by fitting the measured **q** dependence of the inelastic peak position with an empirical quadratic form:

$$\hbar\omega(q_\parallel)=\sqrt{\delta_0^2+c^2q_\parallel^2}. \tag{5}$$

Here $q_\parallel$ denotes the longitudinal component of the wave vector relative to the nearest 3D AF reciprocal-space point, δ_0 is the energy gap at the dispersion minimum, and c is the spin wave velocity along the chains. The resulting fit is shown in Fig. 13 as a solid line. For $T=30$ K the refined value,

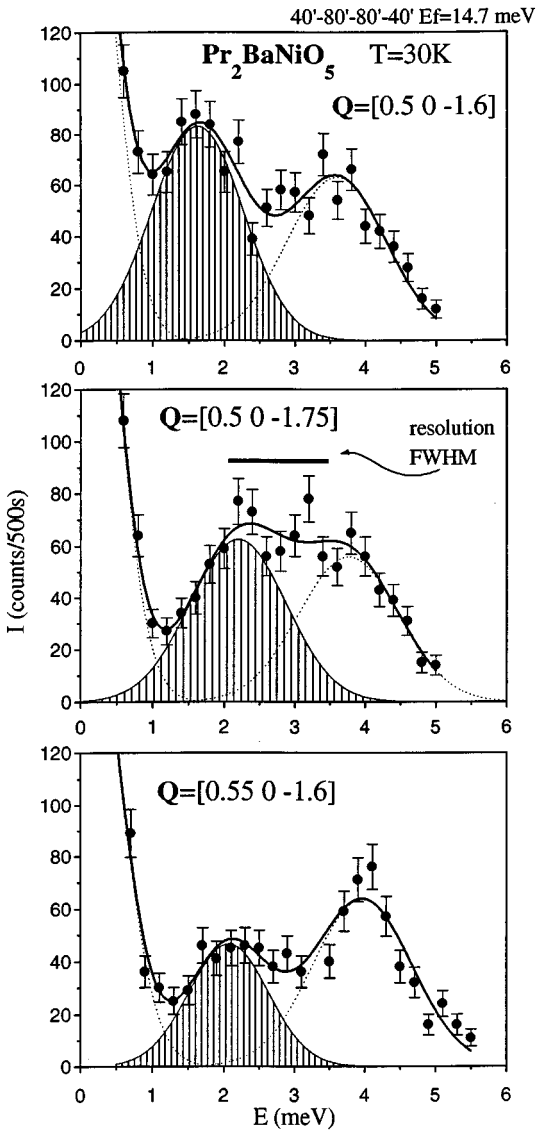

FIG. 11. Example constant-Q scans showing the magnetic-excitons (hatched) and single-ion crystal-field excitations in Pr_2BaNiO_5 at different wave vectors, $T=30$ K. The solid lines represent empirical multiple-Gaussian fits.

$c=30$ meV Å, is substantially smaller than the longitudinal spin-wave velocity c_0 for the Ni-chain modes.

3. Temperature dependence

The dispersion and integrated intensity in the low-energy band were found to be strongly temperature dependent. This is illustrated in Fig. 14, which shows several constant-Q scans collected near the 3D AF point $(0.5,0,-1.5)$. Here the incoherent elastic scattering, represented by a resolution-limited Gaussian-shaped central component at $\hbar\omega=0$, has been subtracted from the experimental data points. The dashed lines show Gaussian fits. As the Néel temperature T_N is approached from above, the gap at $\mathbf{Q}=((2m+1)/2,0,(2n+1)/2)$ decreases [Fig. 10(a)]. At $T=T_N$ the energy gap vanishes; i.e., a complete softening occurs at the 3D AF zone center. The energy-integrated intensity in the low-energy mode decreases rapidly above $T=40$ K and the inelastic peak seems to merge with the one associated with the ''4 meV'' CF transition (Fig. 14). The magnetic-exciton band could not be observed at $T>50$ K.

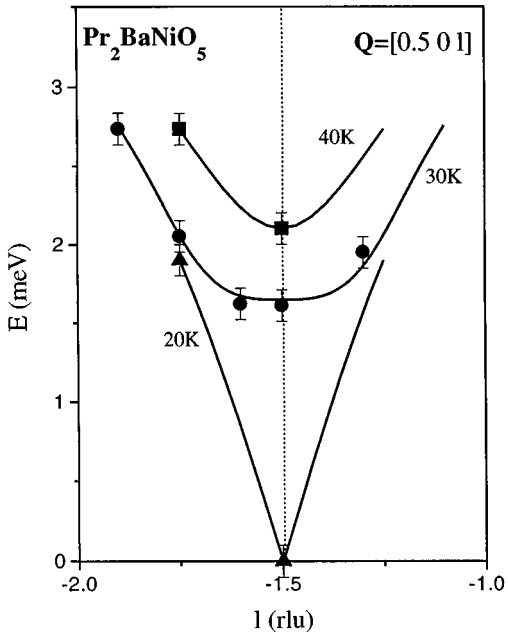

FIG. 12. Measured temperature-dependent dispersion in the magnetic-exciton band perpendicular to the Ni-chain direction in Pr_2BaNiO_5. The solid lines are guides to the eye.

The softening at $((2m+1)/2,0,(2n+1)/2)$ is accompanied by dramatic changes in the whole dispersion branch, as

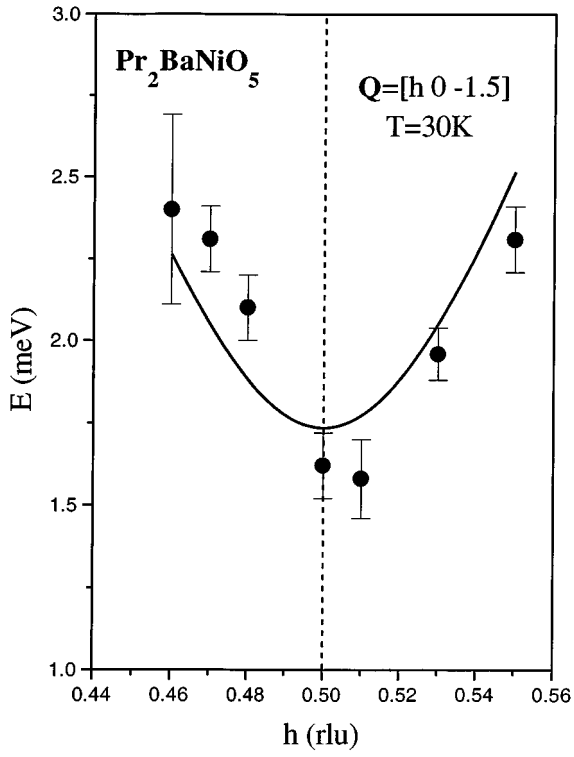

FIG. 13. Measured longitudinal dispersion in the magnetic-exciton band in Pr_2BaNiO_5 at $T=30$ K. The solid line shows an empirical parabolic fit.

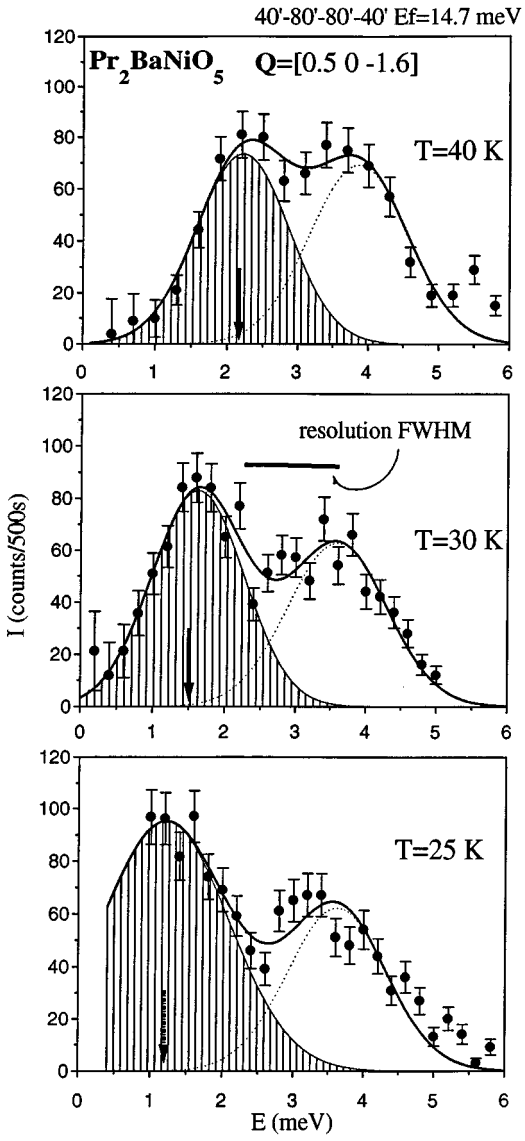

FIG. 14. Example constant-Q scans showing the temperature dependence of the magnetic-exciton (hatched) and single-ion crystal-field branches in Pr_2BaNiO_5 at $T=30$ K. The solid lines are empirical multiple-Gaussian fits. For better visibility the Gaussian-shaped incoherent scattering peaked at $\hbar\omega=0$ has been subtracted from the data.

shown in Fig. 12. This can also be seen from Fig. 10 (solid symbols), which shows the temperature dependence of the excitation energies for several wave vectors. The magnetic-exciton band does not appear as a gap excitation at $T<T_N$. Instead, our results suggest that it is replaced by a conventional gapless spin wave with a linear dispersion around the magnetic Bragg peaks (20 K data in Fig. 12).

IV. DISCUSSION

A. Soft-mode magnetic phase transition

The temperature dependence of magnetic-exciton bands has been extensively studied in Pr metal (Ref. 34 and references therein). If the single-ion excitation energy is δ, then within the random phase approximation (RPA) the band energy is given by[34]

$$(\hbar\omega_{n,\mathbf{q}})^2=\delta^2-2\delta M^2R(T)J_n(\mathbf{q})=\delta^2-\alpha_n(\mathbf{q})R(T), \quad (6)$$

where $J_n(\mathbf{q})$ is the Fourier transform of the appropriate combination of exchange couplings for the nth band, and M denotes the matrix element for the total angular momentum operator between the ground and the excited states. $R(T)$ is a temperature-dependent renormalization factor[35,34] that takes into account the inhibition of excitation hopping (and hence reduction of the bandwidth) as the thermal population of the excitons increases. For a singlet-to-singlet transition model, $R(T)=\tanh(\delta/2kT)$. The temperature dependence observed in the low-energy excitation in Pr_2BaNiO_5 can be entirely understood within this framework. The solid lines in Fig. 10 are fits to Eq. (6) with $\delta=3.85$ meV and the T dependence coming from the renormalization factor R. As the temperature decreases the dip in the dispersion curve deepens and a complete softening eventually occurs at $T=T_N$. This leads to a ''condensation'' of Pr-Ni mixed-spin magnetic excitons and the appearance of finite static moments on both the rare-earth and Ni sites. The magnetic excitons themselves are replaced by conventional Goldstone modes, which reflect the breakdown of translational symmetry in the Néel phase. This scenario is supported by the correlation which exists between inelastic energy-integrated intensities at $T>T_N$ and magnetic Bragg intensities at $T<T_N$.

Although soft-mode magnetic transitions have been previously observed in other compounds such as Pr-Nd alloys[38] and Pr metal under uniaxial stress,[39] it is a rare and unusual mechanism of magnetic ordering. What makes the magnetic transition in Pr_2BaNiO_5 unique is the mixed-spin nature of the driving magnetic-exciton band. The in-chain Ni-Ni exchange interactions are dominant.[40,41] The only feasible exchange pathway which would complete a 3D linkage of the rare-earth ions involves the Ni sites [Fig. 1(b)]. The magnetic excitons are mixed-spin excitations which reflect correlated fluctuations of both Ni and Pr moments.

The coexistence of what appears as a single-ion CF transition in Pr and wideband Pr-Ni mixed-spin excitons is easily rationalized. With 4 Pr ions per chemical unit cell and 16 per magnetic cell, a number of exciton bands derived from the same crystal field excitation may be expected. From this point of view the single-ion CF transition may be viewed as an optical magnetic-exciton branch (or several closely overlapping branches) with little dispersion and propagating predominantly on the Pr sites. This is consistent with the apparent merging of the low-energy and single-ion CF peaks at elevated temperatures: The dispersion in the Ni-Pr magnetic-exciton band is suppressed and the mode becomes indistinguishable from a single-ion CF transition. The temperature dependence of the ''4 meV'' excitation (Fig. 10, open circles) is also perfectly described by Eq. (6), assuming $\delta=3.85$ meV, just like for the magnetic-exciton band.

B. Haldane-like gap excitations in a mixed-spin system

One of the striking results is the apparent independence of at least some of the Ni-chain modes from the mixed-spin magnetic-exciton bands and (at low temperature) the gapless antiferromagnetic spin waves. In fact, this ''decoupling'' of the different branches is a natural consequence of the large anisotropy of exchange constants in the system, the interaction within the Ni-chains being much larger than Ni-Pr and

Pr-Pr coupling.[40,41] The Haldane-like excitation may be viewed as an optical branch in the spectrum of a mixed-spin system, for which the eigenvector has a vanishingly small component on the Pr sites. The central question is whether the Ni-chain modes are a result of the quantum nature of the system and the *integral value* of the Ni^{2+} spin. The similarity of the behavior observed at $T>T_N$ in Pr_2BaNiO_5 to that seen in the quantum-disordered Y_2BaNiO_5 suggests that this is the case. The same conclusion is supported by the fact that the dynamic structure factor is very similar to the one calculated for a Haldane-gap antiferromagnet. To obtain a more convincing proof, a spin-wave theoretical calculation of the magnetic excitation spectrum must be performed and the results directly compared to our neutron scattering data. On the experimental side, further insight may be obtained by performing field-dependent and polarized-neutron measurements and determining the multiplicity and eigenvectors of the Ni-chain modes. These approaches have been very successful in revealing the purely quantum origin of gap excitations in the 3D ordered phases of $CsNiCl_3$ and related $S=1$ compounds,[8–10,24,42] as opposed to ''classical'' modes seen in isostructural half-integer spin systems.[43–45] Our results for Pr_2BaNiO_5 clearly indicate that the observed gap excitation corresponds to fluctuations of spin components perpendicular to the chain direction in the crystal, but it remains unclear whether the mode is a doublet (corresponding to the two transverse Haldane modes) or not. The third component of the Haldane triplet, if present, was not observed. This could be due either to experimetal limitations or to the coupling of the third component to the Pr spins in the magnetic-exciton band.

A clue as to what is going on in the ordered phase may be obtained by carefully considering the temperature dependence of the gap energy and the integrated intensity of the Ni-chain excitations. Let us assume that at $T>T_N$, just like in Y_2BaNiO_5, the observed ≈ 11 meV inelastic peak in Pr_2BaNiO_5 is indeed given by two transverse [polarized in the (b,c) plane] Ni-chain gap modes. In the ordered phase these two branches may no longer be equivalent, since a finite static moment appears on the Ni sites and points roughly along the c crystallographic axis. It is conceivable that the mode polarized along the **c** axis should vanish when the Ni spins become fully ordered. It is known that on cooling through the transition temperature the magnetization on Ni^{2+} sublattices in L_2BaNiO_5 compounds reaches saturation very rapidly and is practically T independent below $T_1 \approx 0.8T_N$ (Refs. 46, 23, 40, and 41). It is roughly in the range $T_N>T>T_1$ that the energy-integrated intensity of the gap modes decreases by a factor of 2 upon cooling, remaining constant at lower temperatures. This may reflect the fact that only one component of the doublet of transverse modes survives long-range ordering. The scenario is consistent with the observed differences in the $Q_\perp$ dependence of the inelastic intensity at 11 meV above and below the ordering temperature: In the ordered phase the peak in a $Q_\perp$ scan appears slightly broader, which may be due to the loss of some intensity originating from **c**-polarized Ni-chain excitations. The suggested picture implies that in the range 20 K $<T<$ 24 K $=T_N$ excitations with both transverse polarizations are present. The one polarized along **c** in this case corresponds to spin fluctuations *along the ordered* Ni^{2+} *moments*. An excitation of a similar nature has been previously observed in the ordered phase of $CsNiCl_3$,[8,9] but is absent in isostructural half-integer spin compounds.[43–45]

The *increase* of the gap in the Ni-chain mode in the ordered phase is a separate result. Theoretical models for 1D gap excitations in $S=1$ antiferromagnetic chains which are part of a 3D mixed-spin system are yet to be developed. It appears though that this peculiar behavior is not related to the soft-mode nature of the magnetic phase transition in Pr_2BaNiO_5. This was confirmed recently in inelastic neutron scattering experiments on Nd_2BaNiO_5 powder samples.[33] In this material Haldane-like Ni-chain gap modes were observed above and below the Néel temperature $T_N=48$ K. The temperature dependence of the energy gap is very similar to that found in Pr_2BaNiO_5. Nd^{3+}, however, is a Kramers ion and its magnetic moment cannot be totally quenched by the low site symmetry. The magnetic transition in Nd_2BaNiO_5 is presumably of a conventional (non-soft-mode) type.

We have shown that the gap in the Ni-chain branch in Pr_2BaNiO_5 continues to increase with cooling at least down to $T=10$ K. As noted above, the Ni^{2+} moments are expected to be saturated below $T=20$ K and therefore the temperature dependence of the gap energy may not be easily explained by the temperature dependence in the Ni-order parameter. One possible scenario for the observed behavior emphasizes the role of Pr-Ni interactions. The L^{3+} order parameter in L_2BaNiO_5 systems, unlike that of Ni^{2+}, increases linearly with decreasing T down to $T \approx 0.2T_N$.[46,23,41] It is plausible that a steady increase in the Pr-sublattice magnetization and the consequent increase of the effective staggered field induced on the Ni sites by Pr^{3+} moments are the driving force for the temperature dependence of the gap. A full understanding of this phenomenon requires new theoretical input.

Considering the temperature dependence of the Ni-chain Haldane-like gap modes in Pr_2BaNiO_5 we find that it is totally different from that in $CsNiCl_3$.[7,8] In the latter compound all three Haldane gap modes present in the 1D phase undergo a complete softening at the transition temperature. The two transverse modes are replaced by conventional gapless magnons (Goldstone modes) in the ordered phase. In contrast, at least some of the Ni-chain gap excitations in Pr_2BaNiO_5 persist as gap modes at $T<T_N$ and do not show any substantial softening at the transition temperature. They have a negligible contribution from Pr and, in consequence, a purely 1D structure factor dependence. These excitations are therefore not related to the Goldstone modes in the ordered phase, which, as discussed above, are seen as separate branches with a cross section that is modulated by a 3D magnetic structure factor. $CsNiCl_3$, on the other hand, has a much simpler spin structure than Pr_2BaNiO_5, with only one type of spin carrier, and it is inevitable that Haldane-gap modes and acoustic spin waves are actually one and the same set of excitations.

V. CONCLUSION

Thanks to the interaction between $S=1$ antiferromagnetic Ni chains and light rare-earth ions, Pr_2BaNiO_5 shows a very

rich and unusual magnetic excitation spectrum. Long-range magnetic order is induced by a softening in a mixed-spin Pr-Ni magnetic-exciton band. Haldane-like gap excitations, propagating predominantly on the Ni sites, persist in the 3D ordered phase. Their temperature dependence is significantly changed when the Néel temperature is crossed.

ACKNOWLEDGMENTS

The authors would like to thank P. Bak, I. Affleck, K. Kakurai, C. Broholm, and P. Böni for numerous illuminating discussions. Work at Brookhaven National Laboratory was supported by the Division of Material Sciences, U.S. Department of Energy, under Contract No. DE-AC02-76CH00016.

[1] F. D. M. Haldane, Phys. Lett. **93A**, 464 (1983).
[2] M. P. Nightingale and H. W. J. Blote, Phys. Rev. B **33**, 659 (1986).
[3] K. Nomura, Phys. Rev. B **40**, 2421 (1989).
[4] O. Golinelli, T. Jolicoeur, and R. Lacaze, Phys. Rev. B **45**, 9798 (1992).
[5] S. V. Meshkov, Phys. Rev. B **48**, 6167 (1993).
[6] L. P. Regnault, I. Zaliznyak, J. P. Renard, and C. Vettier, Phys. Rev. B **50**, 9174 (1994).
[7] W. J. L. Buyers *et al.*, Phys. Rev. Lett. **56**, 371 (1996).
[8] R. M. Morra, W. J. L. Buyers, R. L. Armstrong, and K. Hirakawa, Phys. Rev. B **38**, 543 (1988).
[9] K. Kakurai, M. Steiner, R. Pynn, and J. K. Kjems, J. Phys. Condens. Matter **3**, 715 (1991).
[10] K. Kakurai, Physica B **180-181**, 153 (1992).
[11] J. P. Renard *et al.*, Europhys. Lett. **3**, 945 (1987).
[12] S. Ma *et al.*, Phys. Rev. Lett. **69**, 3571 (1992).
[13] J. P. Renar *et al.*, J. Appl. Phys. **63**, 3538 (1988).
[14] K. Hirota, S. M. Shapiro, K. Katsumata, and M. Hagiwara, Physica B **213**, 173 (1995).
[15] J. P. Renard, L. P. Regnault, and M. Verdaguer, J. Phys (Paris) Colloq. **49**, C8 (1988).
[16] V. Gadet, M. Verdaguer, J. P. Renard, J. Ribas, C. Diaz, M. Montfort, X. Solans, C. P. Landee, J. P. Jamet, and A. Dworkin (unpublished).
[17] A. Zheludev *et al.*, Phys. Rev. B **53**, 15 004 (1996).
[18] J. Darriet and L. P. Regnault, Solid State Commun. **86**, 409 (1993).
[19] J. F. DiTusa *et al.*, Physica B **194-196**, 181 (1994).
[20] J. F. DiTusa *et al.*, Phys. Rev. Lett. **73**, 1857 (1994).
[21] D. J. Buttrey, J. D. Sullivan, and A. L. Rheingold, J. Solid State Chem. **88**, 291 (1990).
[22] E. Garcia-Matres *et al.*, J. Solid State Chem. **103**, 322 (1993).
[23] V. Sachan, D. J. Buttrey, J. M. Tranquada, and G. Shirane, Phys. Rev. B **49**, 9658 (1994).
[24] Z. Tun, W. J. L. Buyers, A. Harrison, and J. A. Rayne, Phys. Rev. B **43**, 13 331 (1991); W. J. L. Buyers, Z. Tun, A. Harrison, J. A. Rayne, and R. M. Nicklow, Physica B **180-181**, 222 (1992).
[25] I. Affleck, Phys. Rev. Lett. **62**, 474 (1989).
[26] I. Affleck and G. F. Wellman, Phys. Rev. B **46**, 8934 (1992).
[27] D. J. Buttrey *et al.* (unpublished).
[28] Throughout this paper reciprocal-space vector components are given in reciprocal-lattice units.
[29] G. Xu, C. Broholm, J. F. DiTusa, G. Aeppli, T. Ito, and H. Takagi (unpublished); C. Broholm (private communication).
[30] T. Yokoo and K. Kakurai (private communication).
[31] T. Yokoo, T. Sakaguchi, K. Kakurai, and J. Akimitsu, J. Phys. Soc. Jpn. **64**, 3651 (1995).
[32] G. E. Bacon, *Neutron Diffraction* (Clarendon Press, Oxford, 1975).
[33] A. Zheludev, J. M. Tranquada, T. Vogt, and D. J. Buttrey, Phys. Rev. B (to be published).
[34] J. Jensen and A. R. Mackintosh, *Rare Earth Magnetism: Structures and Excitations* (Clarendon Press, Oxford, 1991).
[35] J. G. Houmann *et al.*, Phys. Rev. Lett. **34**, 587 (1975).
[36] J. G. Houmann, B. D. Rainford, J. Jensen, and A. R. Mackintosh, Phys. Rev. B **20**, 1105 (1979).
[37] I. W. Sumarlin *et al.*, Phys. Rev. B **51**, 5824 (1995).
[38] B. Lebech, K. A. McEwen, and P.-A. Lingard, J. Phys. C **8**, 1684 (1975).
[39] K. A. McEwen, W. G. Stirling, and C. Vettier, Physica B **120**, 152 (1983).
[40] E. García-Matres, J. L. García-Muñoz, J. L. Martínez, and J. Rodríguez-Carvajal, J. Magn. Magn. Mater. **149**, 363 (1995).
[41] A. Zheludev, J. Hill, and D. Buttrey, Phys. Rev. B (to be published).
[42] M. Enderle, K. Kakurai, M. Steiner, and H. Weinfurter, J. Magn. Magn. Mater. **104-107**, 809 (1992).
[43] A. Harrison, M. F. Collins, J. Abu-Dayyeh, and C. V. Stager, Phys. Rev. B **43**, 679 (1991).
[44] M. Enderle, K. Kakurai, K. N. Clausen, T. Inami, H. Tanaka, and M. Steiner, Europhys. Lett. **25**, 717 (1994).
[45] T. Inami, K. Kakurai, H. Tanaka, M. Enderle, and M. Steiner, J. Phys. Soc. Jpn. **63**, 1530 (1994).
[46] J. A. Alonso *et al.*, Solid State Commun. **76**, 467 (1990).